Macromolecules

pubs.acs.org/Macromolecules Article

Thermomechanical Properties of Solid "Liquid Crystalline" Films from Hot-Pressed Synthetic Polypeptides of Various Macromolecular Architectures

Stephen R. Ekatan, Tianrui Xue, Ziyuan Song, Tianjian Yang, Dennis Ndaya, Montgomery T. Shaw,* Jianjun Cheng,* and Yao Lin*

Cite This: *Macromolecules* 2024, 57, 2008−2018 Read Online

ACCESS | Metrics & More | Article Recommendations | Supporting Information

ABSTRACT: This study revisits the material properties of solid "liquid crystalline" films made from synthetic helical polypeptides and explores their structure−property relationships. Poly(γ-benzyl-L-glutamate) (PBLG) with various molecular weights and architectures (linear, comb-, and brush-like) were transformed into films through mechanical hot pressing. The resulting materials are composed of helical PBLGs arranged in a near-hexagonal lattice, similar to those formed by casting from a concentrated solution in 1,2-dichloroethane (EDC). Despite exhibiting lower apparent crystallinity, these films showed superior mechanical strength, potentially due to the promotion of more interrupted helices and their entanglements under high temperature and pressure. A pronounced chain length effect on the tensile modulus and mechanical strength was observed, aligning with the "interrupted helices" model proposed by us and others. Macromolecules with a polynorbornene (PN) backbone and PBLG side chains mirrored the mechanical and viscoelastic properties of linear PBLGs. Our findings suggest that the folding structures of polypeptide chains and the discontinuity of the folding in longer chains are more influential in determining the macroscopic mechanical properties of the resultant materials than crystallinity, packing ordering, or macromolecular architecture, emphasizing the critical role of cohesive chain network formation in achieving enhanced mechanical strength. This research also presents a versatile approach to fabricating solid-state polypeptide materials, circumventing solubility challenges associated with traditional solution-based processing methods.

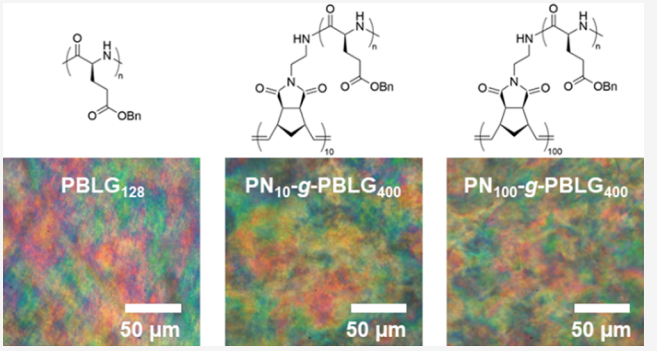

INTRODUCTION

Synthetic polypeptides, through hydrogen bonding, can fold into the ordered secondary structures commonly found in proteins such as α-helices and β-sheets.[1−8] These secondary structures and their well-coordinated interactions can be harnessed to create well-defined supramolecular structures and materials.[9−11] For instance, poly(γ-benzyl-L-glutamate) (PBLG) can form rigid, rod-like α-helices in various organic solvents, leading to a structured, helicoidal supramolecular structure in concentrated solution.[12−14] The cholesteric structure in liquid crystals, retained to an extent in solid films cast from solutions, leads to the formation of unique solid "liquid crystalline" films.[15−19] This concept was originally identified by Tobolsky and Samulski. These films are composed of successive layers of parallel planes, with each plane housing domains of parallel helices. The local liquid crystalline structure endows these films with distinct optical and piezoelectric properties, which are particularly pronounced when the films are oriented under a strong magnetic field.[17−20]

Despite considerable interest in the solid "liquid crystalline" films of synthetic polypeptides, full exploration of their potential applications has been hindered by synthetic challenges. However, recent advancements in the living and accelerated ring-opening polymerization (ROP) of *N*-carboxyanhydrides (NCAs) have facilitated the synthesis of polypeptides with precise control over molecular weights (MWs) and molecular weight distribution (MWD), complex macromolecular architectures, and diverse chemical characteristics.[21−34] The properties of these next-generation synthetic polypeptides are shaped by factors such as their molecular design, conformational structure, packing morphology, side-chain interactions, and the supramolecular organization of the polymer chains. Consequently, it is now timely to systematically assess the potential of the polypeptide "liquid crystalline"

Received: October 2, 2023
Revised: January 28, 2024
Accepted: February 2, 2024
Published: February 21, 2024

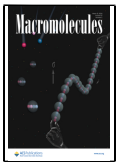

https://doi.org/10.1021/acs.macromol.3c02005
Macromolecules 2024, 57, 2008−2018

films and identify effective and accessible processing strategies to manufacture these materials with high mechanical strengths.

The primary objective of our study is to bolster understanding of the material properties of solid "liquid crystalline" films made from synthetic helical polypeptides, including an investigation of recently synthesized complex-structured polypeptide-containing macromolecules. Past studies have revealed useful observations about helical polypeptides in the solid state but have also left certain questions unresolved. For example, despite the weak molecular interactions between parallel-packed helical rods and a presumably lack of an entangled chain network, these polypeptide films demonstrate considerable mechanical integrity.[12,16,18] This contrasts with coil-like polymers, which typically require a number-average molecular weight (M_n) much higher than the entanglement molecular weight (M_e) to resist fracturing. Previous misconceptions may have originated from the assumption that helical polypeptides existed predominantly as continuous, "single-rod" structures—an idea grounded in the helical cooperativity predicted by Schellman and Zimm.[35−37] However, recent studies suggest that longer helical polypeptides frequently adopt an "interrupted helices" configuration, characterized by multiple helical sequences interspersed with short coil sections.[38−42] This entropy-favored "broken-rod" configuration is observable both in solution and in the melt state, and it is more pronounced when helical polypeptides are incorporated into comb or brush macromolecules due to nonlocal interactions between neighboring grafted chains.[39,42] This structural modification might contribute to a form of the entanglement effect in the melt state, particularly in helical polypeptides of high MWs and under processing conditions that further interrupt the helical chain continuity such as hot-pressing rather than solvent casting. By producing and comparing the material performance of solid films of synthetic polypeptides with various chain lengths and macromolecular architectures, we hope to elucidate how the structural difference between helices and random coils, along with their combinations, contributes to the distinct material properties observed in the solid state.

In this paper, we employ PBLG as a model system to examine the impact of processing conditions, chain length, and macromolecular architecture on the thermomechanical properties of solid "liquid crystalline" films derived from synthetic polypeptides. We explored the direct fabrication of PBLG films, comparing the properties of these compression-molded films with those fabricated using solution-based methods. Our findings reveal a significant impact of PBLG chain length on the tensile modulus and mechanical strength across all three macromolecular architectures (linear, comb-, and brush-like, as shown in Scheme 1), reinforcing the "interrupted helices" model proposed by us and others. This model also offers insights into the superior mechanical strength exhibited by hot-pressed films. The increased discontinuity of the helices in longer PBLG chains, facilitated during the process, aids in the formation of a chain network, thereby enhancing the macroscopic mechanical properties of the resultant materials. Traditionally, the fabrication of helical polypeptide films heavily relied on solution-based processing methods, which encountered solubility limitations when dealing with extreme chain lengths or intricate architectures. Our research circumvents these limitations, providing more flexible fabrication options for these promising materials, especially when future developments involve novel functional polypeptides with intricate side-chain moieties. Therefore, our study not only advances the understanding of the structural characteristics and their impacts on the mechanical properties of synthetic polypeptide films but also paves the way for their broader applications by proposing viable processing strategies.

Scheme 1. Chemical Structure of Synthesized Linear PBLG, Comb-like PBLG, and Brush-like PBLG

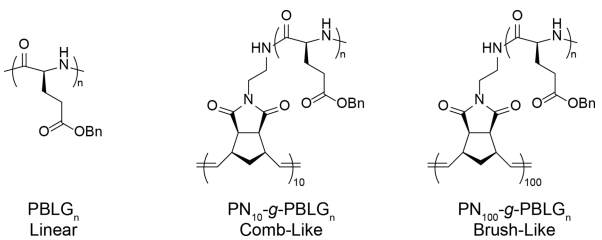

EXPERIMENTAL SECTION

General. All chemicals were purchased from MilliporeSigma (St. Louis, MO, USA) unless otherwise specified. Anhydrous *N*,*N*-dimethylformamide (DMF) was treated with polymer-bound isocyanates (MilliporeSigma, St. Louis, MO, USA) to remove any amine residues, and anhydrous dichloromethane (DCM) was treated with 3 Å molecular sieves and stored at −30 °C in a glovebox. Amino acid, L-glutamic acid γ-benzyl ester, was purchased from Chem-Impex International, Inc. (Wood Dale, IL, USA). Grubbs Catalyst M300 (G3 catalyst) was purchased from MilliporeSigma and stored at −30 °C in a glovebox used for the ring-opening metathesis polymerization (ROMP) of norbornene (NB) monomers. Linear PBLG with viscosity-average molecular weights (M_v) of 32, 82, and 186 kDa was directly purchased from MilliporeSigma and analyzed by GPC (Figure S1). Their number-average molecular weights (M_n) were determined to be 28, 66, and 181 kDa.

Polymer Synthesis and Characterization. Linear PBLG was purchased from the vendor directly. For polynorbornene (PN)-based polypeptides, a PN backbone was used as a scaffold for grafting of helical polypeptides to obtain comb-like and brush-like macromolecules (denoted as PN$_n$-*g*-PBLG$_m$ where *n* and *m* are the designed degree of polymerization (DP) of the PN backbone and the grafted PBLG). The synthesis methodology followed the reported procedures.[26,43,44] A scheme of the synthesis route is shown in Figure S3.

PN polymers were prepared through the ROMP of NB monomers in DCM ($[NB]_0$ = 20 mM; $[NB]_0/[I]_0$ = 10 for comb-like macromolecules, PN$_{10}$-*g*-PBLG$_x$; $[NB]_0/[I]_0$ = 100 for brush-like macromolecules, PN$_{100}$-*g*-PBLG$_x$). The synthesized PN macroinitiators are inherently unstable under ambient conditions. To facilitate GPC analysis, these polymers were protected by capping with Boc groups, following a procedure previously reported by us.[26] The actual DP of the PN backbones was then determined by the number-average molecular weights of the Boc-capped PN polymers, as characterized through GPC analysis.

PN-*g*-PBLG polymers were prepared through ring opening polymerization (ROP) of γ-benzyl-L-glutamate *N*-carboxyanhydride (BLG-NCA) initiated by the PN macroinitiators in either DCM or DMF depending on the expected DP of PBLG. For comb and brush polypeptides at DP 30 and 100, DMF was the solvent for BLG-NCA polymerization ($[NCA]_0$ = 400 mM; $[NCA]_0/[I]_0$ = 30 or 100). For comb and brush polypeptides at DP 400, DCM was the solvent for BLG-NCA polymerization ($[NCA]_0$ = 25 mM; $[NCA]_0/[I]_0$ = 400). The obtained comb or brush polypeptides were purified by precipitation in hexane/ether (1:1, v/v) and were directly analyzed by GPC (Table 1 and Figure S2). The MWs of the PBLG branches were determined by dividing the MWs of the brush polypeptides, as characterized by GPC, by the DP of the PN backbones. These calculated MWs were then utilized to determine the actual DP of the

https://doi.org/10.1021/acs.macromol.3c02005
Macromolecules 2024, 57, 2008−2018

Table 1. Molecular Weights of PBLG-Containing Macromolecules with Comb and Brush Architecture

polymer	M_n[a]/M_n*[b] (kDa)	DP_{PN}[c]	DP_{PBLG}[d]	$Đ$
PN_{10}-g-$PBLG_{30}$	89/65.7	11	37	1.19
PN_{100}-g-$PBLG_{30}$	542/657	98	25	1.18
PN_{10}-g-$PBLG_{100}$	524/219	15	160	1.09
PN_{100}-g-$PBLG_{100}$	4368/2190	150	133	1.05
PN_{10}-g-$PBLG_{400}$	1271/876	11	527	1.07
PN_{100}-g-$PBLG_{400}$	10357/8760	98	482	1.18

[a]M_n is the obtained MWs by GPC. [b]M_n* is the expected MWs calculated based on the designed DP of the PN backbone and grafted PBLG. [c]Calculated DP of the PN backbone. [d]Calculated DP of grafted PBLG.

grafted PBLG chains. This method ensures accurate determination of the molecular characteristics of each PBLG branch within the comb or brush polymer structure.

MW characterization of the linear PBLG and PN and PN-*g*-PBLG polymers was performed by gel permeation chromatography (GPC). All GPC data were collected via an instrument equipped with an isocratic pump (1260 Infinity II, Agilent, Santa Clara, CA, USA), a multiangle static light scattering (MALS) detector with the detection wavelength at 658 nm (DAWN HELEOS-II, Wyatt Technology, Santa Barbara, CA, USA), and a differential refractometer (dRI) detector (Optilab T-rEX, Wyatt Technology, Santa Barbara, CA, USA). Separations were performed by serially connected size exclusion columns (three PLgel MIXED-B columns, 10 mm, 7.5 × 300 mm, Agilent, Santa Clara, CA, USA), which were maintained at a temperature of 40 °C using DMF containing 0.1 M LiBr as the mobile phase at a flow rate of 0.7 mL/min. The MALS detector was calibrated using pure toluene and then was used for the determination of the absolute MWs. All sample solutions were filtered by a 0.45 mm PTFE filter before the injection. The MWs of polypeptides were determined based on the d*n*/d*c* value of each sample calculated offline by using the internal calibration system processed by the software ASTRA 7 (version 7.1.3.15, Wyatt Technology, Santa Barbara, CA, USA).

Film Fabrication. For PBLG films derived from solution-based methods, concentrated solutions of PBLG (15 wt %) in 1,2-dichloroethane (EDC) and DMF were prepared at room temperature. The solutions were allowed to stand without agitation for 24 h to form a homogeneous solution, with EDC solutions kept at room temperature (RT) and DMF solutions kept in an oven at 55 °C. PBLG films were then cast from the concentrated solutions on a Teflon substrate at RT for EDC solutions and 55 °C for DMF solutions. After drying at the respective casting temperature for over 3 h, the films were peeled from the Teflon surface and annealed at 90 °C under vacuum for 24 h to remove the residual solvent. The film preparation procedure was adapted from a protocol used by McKinnon and Tobolsky.[12]

For PBLG films from hot pressing, the mold consisted of two flat plates with shims (0.125 mm) to control the film thickness, while Kapton films served as the release surface. The processing conditions were a temperature of 120 °C and time of 20 min. The thicknesses of the resulting films from both processes were in the range of 100 to 250 μm.

Film Characterization. Analysis of the film structure was performed using wide-angle X-ray scattering (WAXS) and infrared spectroscopy (IR). Wide-angle X-ray patterns were obtained using Ni-filtered Cu Kα radiation from a turnkey Xcalibur PX Ultra diffractometer (Oxford Diffraction) with the Cu X-ray source, 165 mm Onyx CCD detector, and a kappa goniometer. Samples were fixed on a sample holder with the film surface parallel (X-ray beam edge-on). Infrared spectra were measured by use of a Nicolet Magna IR-560 (Nicolet Instrument Corporation) over the region from 400 to 4000 cm^{-1}.

Thermal analysis was performed using the core techniques of thermogravimetric analysis (TGA), differential scanning calorimetry (DSC), and dynamic mechanical analysis (DMA). TGA and DSC analyses were done in a TGA-Q-500 (TA Instruments) and DSC Q-20 (TA Instruments), respectively. Both techniques employed a heating rate of 10 °C/min. DMA measurements were performed with DMA Q-800 (TA Instruments). For viscoelastic properties, measurements were made at a frequency of 1 Hz, strain of 0.1% (determined to be within the linear region of viscoelastic response), and a heating rate of 3 °C/min over the temperature range of 0 to 150 °C. For stress−strain curves, measurements were made at 0 and 40 °C with a force ramp of 0.5 N/min to 18 N using a tension film clamp. At least two replicates were separately prepared. For each replicate, three or more strips were prepared and each was subjected to tensile extension tests at the given temperature. Stress−strain results for each replicate series were averaged. To check for slippage in measurements, two spaced marks were placed on both ends of the films and the two grips were clamped at the centers of the marks. Then, the presence of some part of the marks remaining under their grips after a stress−strain test indicated an absence of slippage.

Polarized optical microscopy (POM) and transmission electron microscopy (TEM) were utilized to analyze the liquid crystalline (LC) ordering in polypeptide films. POM imaging was performed with an Olympus BX50 microscope, featuring crossed-polarizers. For TEM analysis, the Tecnai T12 G2 Spirit BioTWIN microscope operated at 80 kV was employed. The polypeptide films underwent sectioning perpendicular to their surface using an ultramicrotome equipped with a diamond knife (Leica Ultracut UCT), conducted at room temperature to achieve a section thickness of 45 nm. These microtomed sections were then carefully transferred onto copper grids and subjected to staining via exposure to the vapor of a 0.5% RuO_4 aqueous solution for 60 minutes, in preparation for TEM imaging.

RESULTS AND DISCUSSION

Characterization of PBLG "Liquid Crystalline" Films. Tobolsky and others investigated the structure and properties of PBLG films cast from various solvents, proposing three distinct modifications: Form A, Form B, and Form C.[12,14,45] In our study, we included Form B (cast from DMF at elevated temperature) and Form C (cast from EDC) and compared them with compression-molded films. We first examined PBLG homopolymers with progressively increasing chain lengths. For longer chains, PBLG tends to form multiple helical sections interspersed with short coil sections. The critical chain lengths required to produce such interrupted helices (as low as 40−50 repeats) are significantly smaller than those estimated based on Zimm's model.[35,41] We prepared PBLG films with an average DP of 128 (28 kDa), 301 (66 kDa), and 826 (181 kDa) through solution casting using EDC and DMF solvents, as well as hot pressing, as detailed in the experimental section. FTIR spectra of thin PBLG films (Figure S4) showed peaks at 1650 (amide I) and 1545 cm^{-1} (amide II), suggesting an α-helical conformation, irrespective of the chain length or process method.[46] Small quantities of random-coil regions are typically challenging to detect in FTIR spectra.

Polarized optical microscopy (POM) revealed that the DMF-cast polypeptide films (Figure 1a) and EDC-cast films (Figure 1b) primarily exhibit nematic liquid crystalline textures. However, films created by hot pressing (Figure 1c) exhibited distinct iridescent colors, signaling cholesteric liquid crystalline ordering, at least locally. This is a helical arrangement of nematic layers. TEM analysis of hot-pressed PBLG films (Figure 1f), sectioned perpendicularly, revealed a highly distorted cholesteric structure due to thermomechanical processing. In contrast, TEM images of DMF (Figure 1d) and EDC (Figure 1e) cast films showed no cholesteric banding, consistent with POM results and Pochan and Deming's study[23] on nematically ordered PBLG films.

https://doi.org/10.1021/acs.macromol.3c02005
Macromolecules 2024, 57, 2008−2018

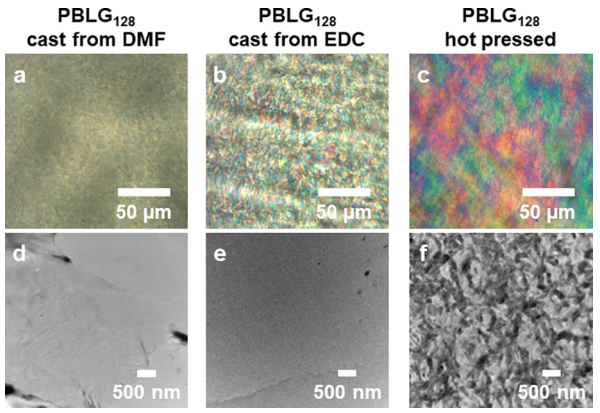

Figure 1. (a–c) POM images of $PBLG_{128}$ films cast from DMF (a), from EDC (b), and prepared via hot pressing (c), respectively. (d–f) TEM images of microtomed $PBLG_{128}$ films cast from DMF (d), from EDC (e), and prepared via hot pressing (f), respectively. Each image showcases the microstructural variations influenced by different processing methods.

Figure 2 shows X-ray diffraction patterns of PBLG films with the X-ray beam edge-on to the film surface (edge view) to reveal the uniplanar orientation of helical chains parallel to the film surface. The sharp equatorial reflections from the films cast from DMF (Figure 2a–c) were indexed by a two-dimensional oblique cell with a = 15.5–15.8 Å, b = 13.1–13.5 Å, and γ = 114–115° (Form B), akin to previous reports by Uematsu (Table S4).[14] The unequal cell edges for Form B were attributed to the distortion of the side chain, which causes the helical chains to deviate from cylindrical symmetry. The films cast from EDC (Figure 2d–f) shows a near-hexagonal packing (Form C), with the cell dimensions as a = 14.7–15.0 Å, b = 14.3–14.7 Å, and γ = 120°, which aligns with previous reports (Table S2).[12] The X-ray diffraction patterns of films made by hot pressing (Figure 2g–i) bear similarity to those cast from EDC, albeit with reduced sharpness, presumably due to the divergent flow during hot pressing. Hereafter, the solid-state modification of films by hot pressing is referred as Form C′. In the diffraction patterns taken with X-ray beam normal to the film surface (through view), the equatorial reflections in Figure 2 appear as Debye–Scherrer rings (Figure S7). This confirms that the helical chains lie in the plane of the film with their helix axes randomly oriented in the plane, indicating a uniplanar orientation.

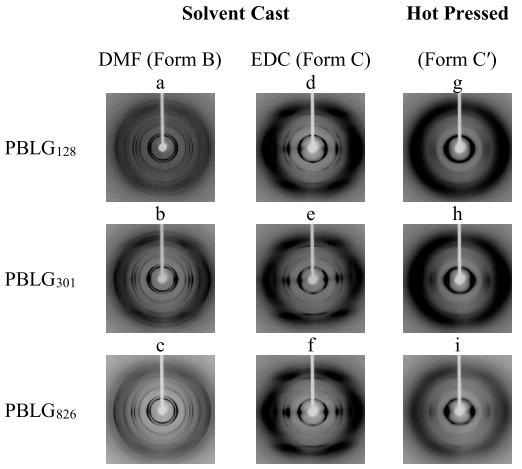

Figure 2. X-ray diffraction patterns of PBLG films. The images were recorded with the film surface parallel to the incident X-ray beam (edge view). (a–c) PBLG films cast from DMF. (d–f) PBLG films cast from EDC. (g–i) PBLG films hot pressing.

The structure of PBLG films is typically interpreted in terms of coexisting paracrystalline and mesomorphic regions. In all three forms, the packing ordering in the films slightly improves with the increasing chain length. Figure S6 shows the apparent crystallinities obtained from analyzing the X-ray diffraction patterns by using a standard method. However, these values should only serve as a relative measure of the molecular ordering in these solid "liquid crystalline" films. Generally, the effectiveness of the processing methods in promoting crystallinity follows the order: DMF (Form B) > EDC (Form C) > hot pressing (Form C′). The unequal cell edges in Form B were found to result from the alternating arrangement of "up" and "down" helices. Uematsu demonstrated through oriented films that Bragg reflections in Form B can be accounted for by a monoclinic unit cell containing two chains, with opposite chain directions, arising from an antiparallel "side-by-side" aggregation of helices in DMF.[14] In contrast, for Form C, the placement of helices appears to be more random, leading to a near-hexagonal lattice. The orientation and side-chain interactions of helices define the packing morphology and ordering in the solid-state modifications.

Thermogravimetric analysis (TGA) measurements indicated no notable weight change attributed to volatiles (Figures S8–

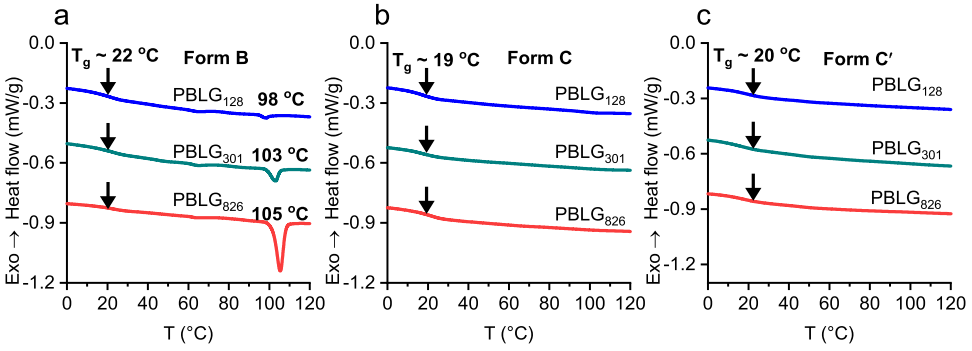

Figure 3. DSC thermograms on first heating for films processed from linear PBLG with three different chain lengths. (a) cast from DMF (Form B), (b) cast from EDC (Form C), and (c) from hot pressing (Form C′). The chain lengths are $PBLG_{128}$ (blue), $PBLG_{301}$ (green), and $PBLG_{826}$ (red). Heating rate of 10 °C/min.

https://doi.org/10.1021/acs.macromol.3c02005
Macromolecules 2024, 57, 2008–2018

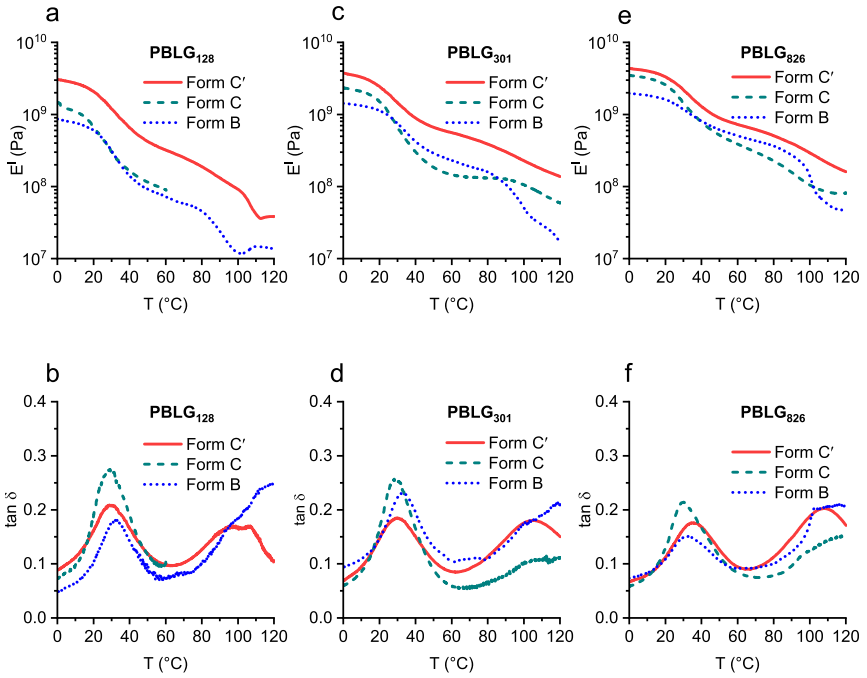

Figure 4. Tensile storage modulus E' and tan δ as a function of temperature for the three different solid-state modifications of the films with DP of 128 (a, b), 301 (c, d), and 826 (e, f). The measurements were carried out at a frequency of 1 Hz. Form B in (a) fractured at ∼60 °C.

S11). Nevertheless, films derived from solutions may retain residual solvents that might be undetectable via TGA. The residual solvent could potentially function as a plasticizer or enhance interchain interactions, thereby altering the viscoelastic properties of the film (Figure S15). Therefore, we exercised additional caution to eliminate the residual solvent from all the films. We noted a significant increase in the temperature of decomposition with the increment in chain length, while the onset temperature for decomposition seemed to be independent of the PBLG form (Figure S16).

In DSC traces shown in Figure 3, all PBLG films display a glass-like transition (T_g) near 20 °C. This transition in PBLG has traditionally been associated with the onset of side-chain motions in the mesomorphic regions.[12,45] However, given that interrupted helices, as opposed to an "all-helix" structure, should now be taken into consideration for PBLG in the films, this glass transition may also involve the segmental motion of the short coils that connect the helical segments. The consistent occurrence of this transition at roughly the same temperature across all PBLG forms suggests that the onset of side-chain movements is not influenced by the packing, processing method, or chain length. An endothermic peak at approximately 100 °C is observed in Form B, although it is barely noticeable in Form C and completely absent in Form C′ (Figure 3). The heat of transition of this peak significantly increases with chain length (0.4 for $PBLG_{128}$, 1.3 for $PBLG_{301}$, and 6.8 J/g for $PBLG_{826}$). This endothermic peak may be associated with a disruption of stacked phenyl rings in the side chain of PBLG in the paracrystalline region.[47,48] Following dissociation, the phenyl rings do not restack upon cooling, as inferred from the lack of an endothermic peak in a second heat cycle (Figure S18). The orderly arrangement of the benzyl group at the end of the side chain seems to require the antiparallel aggregation of α-helices with a more favorable dipole−dipole interaction, which is far more prevalent in Form B than Form C. The relatively poor orientation correlation in Form C likely results from the tendency to form PBLG aggregates in EDC, which subsequently induces more interrupted helices with increased disorder. In contrast, PBLG is well dispersed in DMF and only forms well-defined, rod-like assembly of helices in concentrated solutions (e.g., 40 wt %). The subsequent DMA analysis revealed the impact of different molecular associations and structures on the viscoelastic properties of the films.

Thermomechanical Properties of PBLG Films. Figure 4 illustrates the dependency of the viscoelastic behaviors of films on the form and DP of PBLG. All films exhibit a decrease in modulus near 30 °C, aligning with the glass-like transition observed in DSC. The modulus decrease in this transition is relatively modest in Form B compared to Form C possibly due to the phenyl-ring interactions in Form B. Furthermore, the higher the DP, the less pronounced the decrease in modulus in Form B. It seems that the degree of restraint from the phenyl-ring interaction escalates with the chain length, as evidenced by their measured heat of transition in DSC. Upon the dissociation of the phenyl-ring stack in the side chain, Form B exhibits a significant modulus transition at ∼90 °C, with a large decrease in modulus for all three DPs. It has been previously demonstrated that the packing of the PBLG chains transitions from pseudohexagonal to a hexagonal lattice at 95 °C, where the side chains can now experience free motion even in the paracrystalline region.[4]

For all three forms, modulus increases substantially with DP. Notably, Form C′ exhibits a higher modulus at all temperatures between 0 and 120 °C compared to either Forms B or C. Despite being structurally similar to Form C cast from EDC, as evidenced by the X-ray diffraction patterns in Figure 2, Form C′ from hot pressing exhibit significantly reduced ordering. Given that polymer crystallization often provides mechanical reinforcement for semicrystalline polymers with low T_g, it might seem counterintuitive that the films with more mesomorphic and probably disordered regions, and devoid of

https://doi.org/10.1021/acs.macromol.3c02005
Macromolecules 2024, 57, 2008−2018

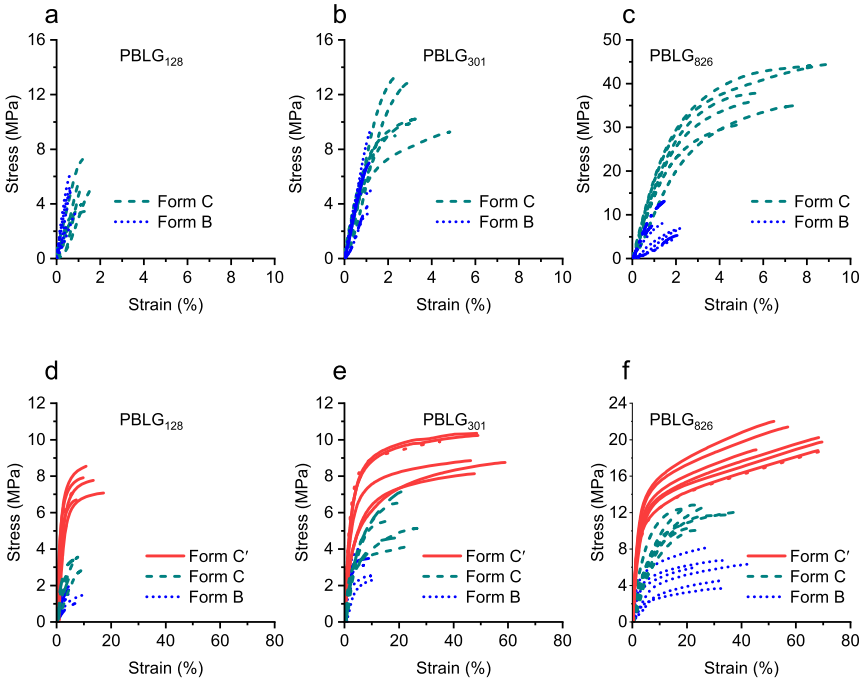

Figure 5. Tensile stress−strain curves of PBLG films. (a−c) at 0 °C and (d−f) at 40 °C. Form C′ was not run at 0 °C.

phenyl-ring interactions, exhibit the highest modulus across a wide temperature range. However, the cohesive strength of a polymer film is determined by both amorphous and crystalline regions and importantly, the structural connectivity between them, that is, chain networking. A highly crystalline film may be weak if the chain network is largely absent. On the other hand, a partially crystallized film with dispersed crystalline and amorphous regions may possess structural connectivity and intermolecular chain uncrossability, thereby providing the material with cohesive strength.[49,50] For PBLG of sufficiently high molecular weight, the formation of interrupted helices, partially in the paracrystalline domain and partially in the mesomorphic domain, should establish a robust chain network through topological entanglement. Especially, the presence of short segments of coils in "interrupted" helical structures could potentially lead to some form of topological entanglement in melts and affect mechanical properties, an effect that is more pronounced with high DPs and low packing order (e.g., Form C′). Consequently, we conducted tensile tests on the films at temperatures both below and above the T_g, to examine the dependency of ductility on the chain length, which is presumed to increase the chain network density.

Tensile Strength and Ductility of PBLG Films. The stress−strain curves are presented in Figure 5. At 0 °C (~20 °C below the glass-like transition), Form C′ was too rigid to extend, causing film slippage in the sample holder; hence, only the results from Form B and Form C were included. At 40 °C (~20 °C above the glass-like transition), all three Forms were examined. The stress−strain curves in Figure 5 were processed to extract the values of elongation at break and strength at break. A summary of the stress−strain behavior is shown in Figure 6. Linear regression analysis using Minitab software confirmed the statistical significance (p statistic) of the results, such as the impact of chain length and processing method on the percentage elongation at break and strength at break (see SI for the detailed statistical analysis and discussions).

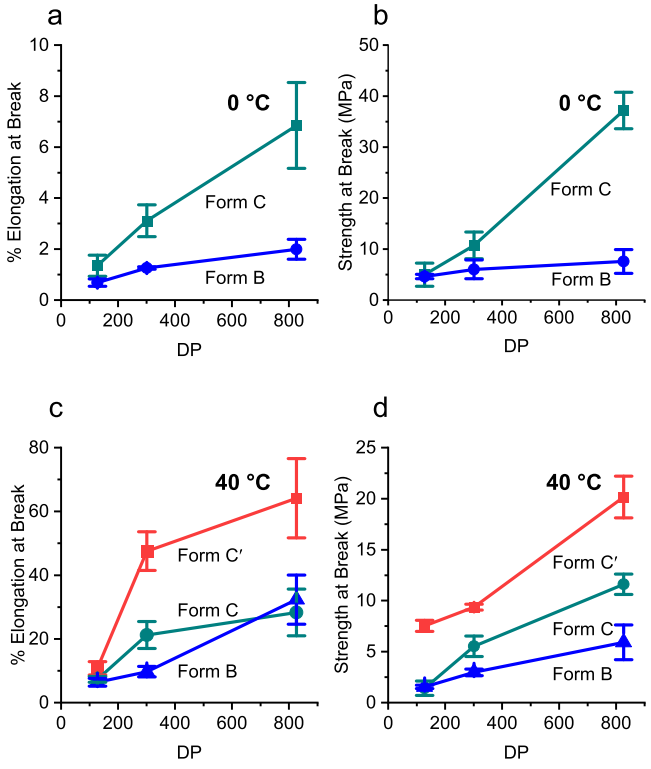

Figure 6. Summary of stress−strain behavior for stress−strain curves shown in Figure 5. (a, b) at 0 °C and (c, d) at 40 °C. Left to Right; % elongation at break and strength at break, respectively.

At both temperatures shown in Figure 6, the correlation between the chain length and both percentage elongation at break and strength at break (or breaking stress) is statistically significant for all the tested forms (see SI and Tables S5−S12). A temperature increase from 0 to 40 °C correlates with a considerable increase in percentage elongation at break and a

https://doi.org/10.1021/acs.macromol.3c02005
Macromolecules 2024, 57, 2008−2018

decrease in breaking stress, corroborating the glass-like transition observed in both DSC and DMA.

Under tensile extension, PBLG films exhibit brittleness below the glass transition temperature (T_g). Interestingly, high DP Form C is more drawable than either Form B or low DP Form C. From our previous studies, we know that the critical DP facilitating interrupted helices of synthetic polypeptides is relatively short in solvents like chloroform and EDC (as low as 40−50).[40−42] PBLG with longer chains typically exists as interrupted helices interspersed with scattered coil sections. For semicrystalline polymers in a glassy state, the cohesive strength is largely determined by the density of intermolecular chain uncrossability. Thus, casting films from high DP PBLG and using solvent conditions that favor interrupted helical structures can enhance the formation of a chain network through topological entanglement.

Above T_g, the drawability and mechanical strength of Form C′ significantly surpasses that of Forms B and C. The enhancement in drawability and strength in polymers with high DP is a common phenomenon in melts of Gaussian-chain polymers, which are treated as an entangled chain network. An increase in the chain length results in a greater number of entanglements, making these entanglements more resistant to failure by slippage or disentanglement during stress−strain analysis, thus yielding higher tensile strength. In PBLG films, the interrupted helices from the solution phase likely persist and may even intensify under hot pressing. Solution-cast films allow partial disentanglement and orientation during drying, whereas hot pressing enhances entanglement due to radial flow. Consequently, Form C′ demonstrates markedly higher breaking strength than Forms B and C, attributed to the forced entanglement during hot pressing.

Characterization of "Liquid Crystalline" Films Made by Comb- and Brush-like PBLGs. We proceeded to examine polynorbornene-*graft*-PBLG macromolecules (PN_x-*g*-$PBLG_n$, x and n are the DP of PN backbone and PBLG grafts, respectively). These grafted PBLGs in such macromolecules have more pronounced structural interference due to local crowding and interactions between neighboring chains. Six polymers were synthesized and characterized using previously developed methods (Figures S2 and S3). We designated the series of PN_{10}-*g*-$PBLG_n$ (n = 30, 100, and 400) as comb-like macromolecules, while the series of PN_{100}-*g*-$PBLG_n$ (n = 30, 100, and 400) was called brush-like macromolecules. Films of these polymers were prepared via compression molding and subsequently annealed at 90 °C for 12 h to remove any residual solvent. TGA conducted on these films did not show any weight loss attributed to volatiles (Figures S12−S14). FTIR spectra of thin films of the PN_x-*g*-$PBLG_n$ polymers (Figure S5) showed peaks at 1650 (amide I) and 1545 cm^{-1} (amide II), indicating a predominantly α-helical conformation, regardless of the side chain or backbone length.[26] The POM images (Figure 7) of hot-pressed films from both comb- and brush-like PBLGs display iridescent colors, akin to those observed in linear PBLGs, indicative of localized cholesteric liquid crystalline supramolecular structures.

The X-ray diffraction patterns of the PN_x-*g*-$PBLG_n$ films, obtained with X-ray beam edge-on and normal to the films, are shown in Figure 8. These patterns primarily consist of a few rings superimposed on a diffuse background. The diffraction patterns show a significant amount of diffuse scattering and lack sharp reflections in both the equatorial and meridional directions. Such observations indicate that these films have low

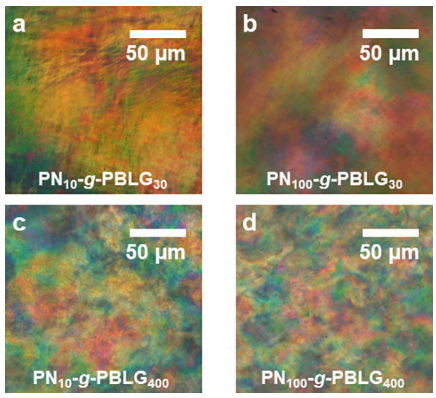

Figure 7. POM images of comb-like and brush-like PBLG films prepared from hot pressing. (a) PN_{10}-*g*-$PBLG_{30}$ films. (b) PN_{100}-*g*-$PBLG_{30}$ films. (c) PN_{10}-*g*-$PBLG_{400}$ films. (d) PN_{100}-*g*-$PBLG_{400}$ films.

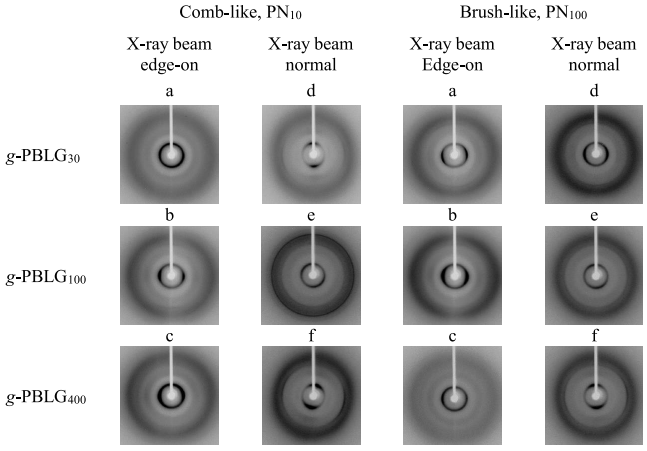

Figure 8. X-ray diffraction patterns of hot-pressed films of comb-like and brush-like macromolecules. (a−c) Film surface is parallel to the incident X-ray beam (edge view). (d−f) Film surface is normal to the incident X-ray beam (normal view).

apparent crystallinity and reduced orientation, compared to PBLG films. This is likely due to the limited mobility of the grafted PBLGs, covalently bound to the PN backbone in the comb- or brush-like macromolecules, hindering the formation of paracrystalline and mesomorphic regions in the hot-pressed samples.

In DSC traces (Figure 9), all films exhibit a glass-like transition at around 20 °C, mirroring the observations made in PBLG homopolymers.[21,22] The consistency of this transition across all PN-*g*-PBLG samples suggests that the side-chain motions of the grafted PBLGs are unaffected by changes in macromolecular architecture or crystallinity. Interestingly, an endothermic peak around 90 °C is observed in the DSC traces, which is absent in the second heat cycle (Figure S20). A similar peak, though of higher magnitude, was observed in the Form B homopolymer. The molecular associations contributing to this peak likely share the same origin as those in Form B. The interdigitation of neighboring PN-*g*-PBLGs may facilitate the antiparallel packing of grafted PBLGs and stacking of the phenyl rings. However, the degree of phenyl ring stacking is significantly less than that observed in Form B processed through solvent casting. The influence of these molecular associations on the viscoelastic properties of the

https://doi.org/10.1021/acs.macromol.3c02005
Macromolecules 2024, 57, 2008−2018

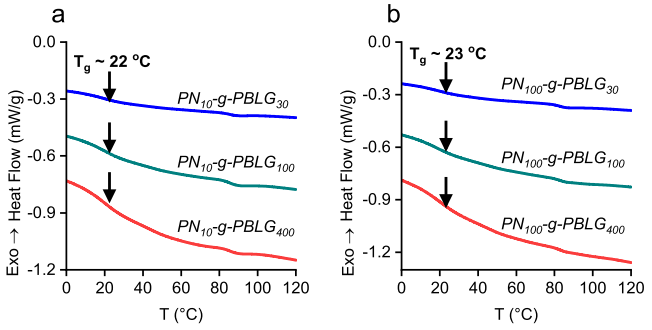

Figure 9. DSC thermograms on first heating for hot-pressed films of comb-like and brush-like macromolecules with three different PBLG graft chain lengths. (a) Comb-like and (b) brush-like. The graft chain lengths are $PBLG_{30}$ (blue), $PBLG_{100}$ (green), and $PBLG_{400}$ (red). Heating rate of 10 °C/min.

comb- and brush-like macromolecules containing PBLG grafts is revealed in the DMA analysis, presented in Figure 10.

Mechanical Properties of PN-*g*-PBLG Films. Figure 10 shows how the viscoelastic behavior of films depends on the grafted and backbone chain length of the comb- and brush-like PN-*g*-PBLGs. All films exhibit a decrease in modulus beginning at 20 °C, consistent with the glass-like transition identified in the DSC results. As observed in linear PBLGs, the tensile storage modulus is influenced by the PBLG chain length. The longer the grafted PBLGs, the higher the modulus, indicating an entanglement-like behavior of long helical chains. Intriguingly, both the comb macromolecules (PN_{10}-*g*-$PBLG_n$) and brush macromolecules (PN_{100}-*g*-$PBLG_n$) have tensile storage moduli comparable to their linear PBLG equivalents ($PBLG_n$). This sharply contrasts with the polymers of random coils, where macromolecular architectures can play a highly significant role. For instance, in brush-like polymers grafted with coil-like chains, steric interactions and crowding of grafted chains cause the straightening of grafted chains and a minimal extent of entanglements in these polymers.[51−53] Lately, Sheiko's work shows that the modulus of conventional molecular brushes can be as low as 100 Pa, highlighting their capability to form supersoft elastic materials with high strain at break.[54] In the case of PN-*g*-PBLGs, the helical PBLGs are already "stretched" and compact. Hence, the interactions and packing morphology of grafted PBLGs determine the mechanical properties of the resulting materials. Previously, we demonstrated that high molecular weight grafted PBLGs in comb- or brush-like macromolecules tend to fragment into interrupted helices with short coil segments between helices.[40−42] These more interrupted grafted chains are prone to entanglement with each other, contributing to the increased tensile moduli observed in the comb and brush macromolecules containing longer PBLGs (Figure 10). Additionally, the PN backbone may act as a cross-linker, providing an extra barrier against disentanglement and chain crossability. To explore these hypotheses, we performed tensile tests on the hot-pressed PN-*g*-PBLG films at a temperature above T_g. This allowed us to examine the film's ductility dependence on the DP of PBLG and the macromolecular architecture (Figure 11).

The stress−strain curves in Figure 11 were used to extract the percent elongation at break and tensile strength at break (Figure 12). The increase in both percent elongation at break and strength at break with the DP of the grafted PBLG is statistically significant in both PN_{10}-*g*-$PBLG_n$ and PN_{100}-*g*-$PBLG_n$ but is insignificant when different macromolecular

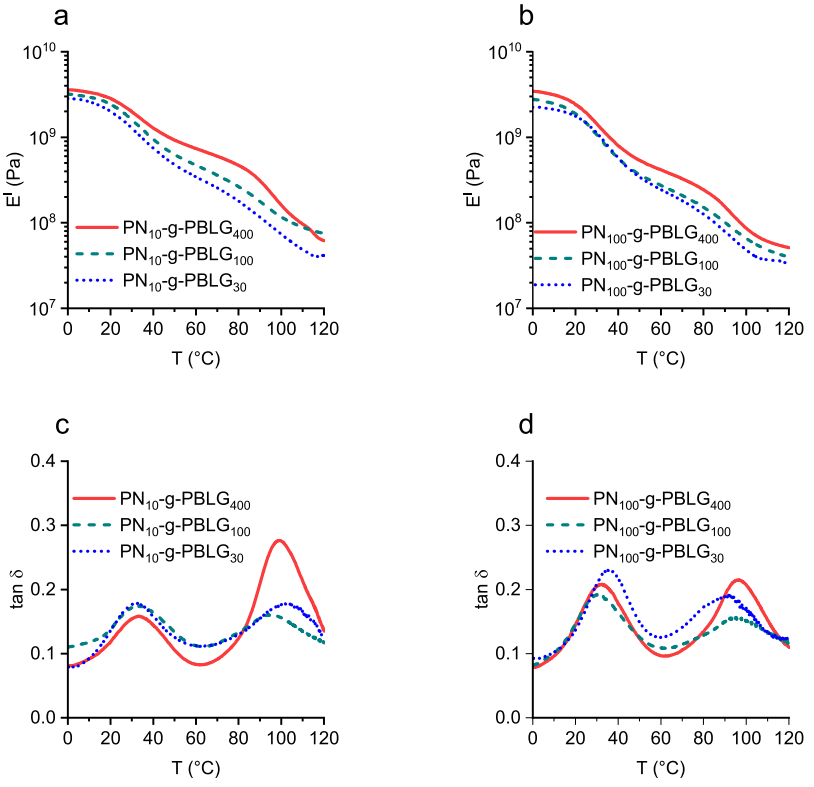

Figure 10. Tensile storage modulus E' and tan δ as a function of temperature for hot-pressed films of comb-like and brush-like macromolecules at a frequency of 1 Hz. (a, b) E' and (c, d) tan δ. Comb-like (a, c) and brush-like (b, d).

https://doi.org/10.1021/acs.macromol.3c02005
Macromolecules 2024, 57, 2008−2018

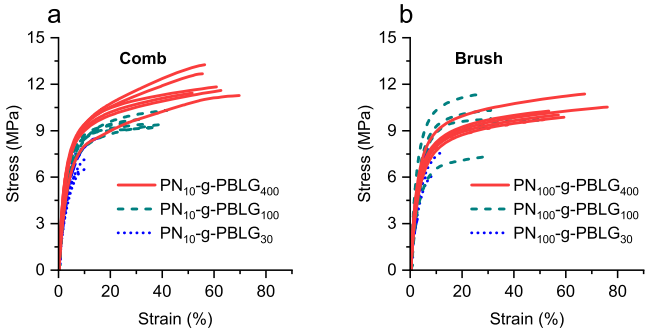

Figure 11. Tensile stress−strain curves of the hot-pressed comb and brushes at 40 °C. (a) Comb and (b) brush.

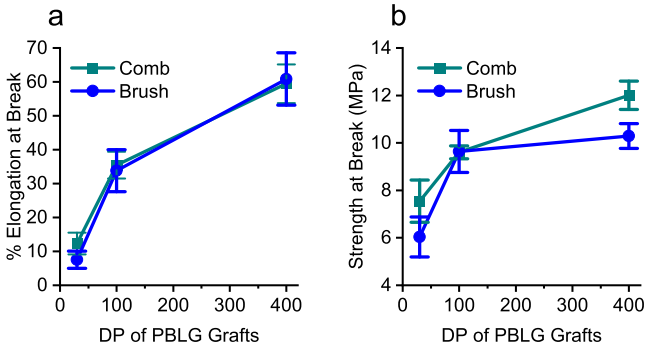

Figure 12. Summary of stress−strain behavior for stress−strain curves shown in Figure 11: (a) % elongation at break and(b) strength at break.

architectures are compared (see SI and Tables S13−S16 for a detailed statistical analysis). Like the linear PBLGs, the enhanced ductility due to the chain length of grafted PBLG is a result of entanglement-like behavior of the interrupted helical chains in the film. This effect is somewhat reinforced by the cross-linking effect of the PN backbone. As in the absence of a PN backbone, films made from a homopolymer of PBLG with DP less than 50 are too fragile for tensile testing as the chains are too short to form adequate entanglement. These findings compellingly demonstrate that the cohesive strength of a polypeptide film is largely dictated by the structural connectivity in a chain network, rather than the apparent crystallinity or local packing ordering.

Kramer and colleagues previously established the critical role of the number-average molecular weight (M_n) in determining the strain level at which a polymer will fracture, as manifested in its elongation at break.[51] Typically, coil-like polymers require an M_n at least 2 to 3 times that of the entanglement molecular weights (M_e) to possess sufficient mechanical strength for fracture properties to be measurable.[55] With an increase in M_n, an increment in the elongation at break is observed until a saturation point is reached when M_n exceeds ∼20 times the M_e. This pattern remains consistent for linear PBLG, presuming an M_e equivalent to the average molecular weight of continuous helical segments (approximately ∼40 repeating units)[40−42] and for the three PBLG samples where M_n/M_e is then around 3, 10, and 20. Intriguingly, both comb and brush PBLGs, when accounting for the DP of grafts, adhere to this general trend. This observation reaffirms the critical role of the PBLG chain length and the "broken-rods" nature of these helical polymers in governing the fracture behavior of the compression-molded films, with their macromolecular architectures exerting a significantly lesser impact.

CONCLUSIONS

Utilizing PBLG as an experimental model system for helical polypeptides, we have explored how solid "liquid crystalline" films with robust mechanical strengths may be created by compression molding the polymers at temperatures significantly above their T_g. PBLGs of different MWs and macromolecular architectures (linear, comb-, and brush-like) were readily shaped into bulk materials through mechanical hot pressing. Despite the lower apparent crystallinity of the hot-pressed samples, the helical PBLGs in these materials were packed on a near-hexagonal lattice, exhibiting superior mechanical strength compared to films prepared by solvent casting. The noticeable effect of the chain length on the tensile modulus and mechanical strength, irrespective of macromolecular architecture, suggests that forming a cohesive chain network via chain entanglement is central to achieving robust mechanical properties in these synthetic polypeptides with defined secondary structures. In cases where the helical chain is too short to entangle, a "cross-linking" effect from the PN backbone in a comb- or brush-like macromolecular architecture, combined with the interdigitation of grafted helices, can aid in the formation of the requisite chain network for substantial mechanical strength. Contrary to expectations, it is the folding structures of polypeptide chains and the discontinuity of the folding in longer chains, such as interrupted helices, that determine the macroscopic mechanical properties of the resulting materials rather than the crystallinity or packing ordering of the helical chains. The "interrupted helices" model proves particularly enlightening in understanding the entanglement-like behavior observed in these polypeptide materials.

ASSOCIATED CONTENT

Supporting Information

The Supporting Information is available free of charge at https://pubs.acs.org/doi/10.1021/acs.macromol.3c02005.

GPC chromatograms; FTIR spectra; WAXS patterns; TGA and DSC thermograms; DMA temperature sweeps; replicates of various thermomechanical experiments; statistical analysis (PDF)

AUTHOR INFORMATION

Corresponding Authors

Montgomery T. Shaw − *Polymer Program, Institute of Materials Science and Department of Chemical & Biomolecular Engineering, University of Connecticut, Storrs, Connecticut 06269, United States*; Email: montgomery.shaw@uconn.edu

Jianjun Cheng − *Department of Materials Science and Engineering and Department of Chemistry, University of Illinois at Urbana−Champaign, Urbana, Illinois 61801, United States*; orcid.org/0000-0003-2561-9291; Email: jianjunc@illinois.edu

Yao Lin − *Polymer Program, Institute of Materials Science and Department of Chemistry, University of Connecticut, Storrs, Connecticut 06269, United States*; orcid.org/0000-0001-5227-2663; Email: yao.lin@uconn.edu

https://doi.org/10.1021/acs.macromol.3c02005
Macromolecules 2024, 57, 2008−2018

Authors

Stephen R. Ekatan − *Polymer Program, Institute of Materials Science, University of Connecticut, Storrs, Connecticut 06269, United States*

Tianrui Xue − *Department of Chemistry, University of Illinois at Urbana−Champaign, Urbana, Illinois 61801, United States*

Ziyuan Song − *Department of Materials Science and Engineering, University of Illinois at Urbana−Champaign, Urbana, Illinois 61801, United States;* orcid.org/0000-0002-3165-3712

Tianjian Yang − *Polymer Program, Institute of Materials Science, University of Connecticut, Storrs, Connecticut 06269, United States*

Dennis Ndaya − *Polymer Program, Institute of Materials Science, University of Connecticut, Storrs, Connecticut 06269, United States;* orcid.org/0000-0001-5901-1351

Complete contact information is available at: https://pubs.acs.org/10.1021/acs.macromol.3c02005

Author Contributions

The manuscript was written through contributions of all authors. All authors have given approval to the final version of the manuscript.

Notes

The authors declare no competing financial interest.

■ ACKNOWLEDGMENTS

This research was supported by NSF (DMR-1809497 and DMR 2210590 to Y.L.; CHE-1905097 to J.C.) and GAANN Fellowship No. P200A150330.

■ REFERENCES

(1) Kricheldorf, H. R. Polypeptides and 100 years of chemistry of α-amino acid *N*-carboxyanhydrides. *Angew. Chem., Int. Ed.* **2006**, *45* (35), 5752−5784.

(2) Leigh, T.; Fernandez-Trillo, P. Helical polymers for biological and medical applications. *Nature Reviews Chemistry* **2020**, *4* (6), 291−310.

(3) Deming, T. J. Synthetic polypeptides for biomedical applications. *Prog. Polym. Sci.* **2007**, *32* (8−9), 858−875.

(4) He, C.; Zhuang, X.; Tang, Z.; Tian, H.; Chen, X. Stimuli-Sensitive Synthetic Polypeptide-Based Materials for Drug and Gene Delivery. *Adv. Healthcare Mater.* **2012**, *1* (1), 48−78.

(5) Lu, H.; Wang, J.; Song, Z.; Yin, L.; Zhang, Y.; Tang, H.; Tu, C.; Lin, Y.; Cheng, J. Recent advances in amino acid *N*-carboxyanhydrides and synthetic polypeptides: chemistry, self-assembly and biological applications. *Chem. Commun.* **2014**, *50* (2), 139−155.

(6) Deng, C.; Wu, J.; Cheng, R.; Meng, F.; Klok, H.-A.; Zhong, Z. Functional polypeptide and hybrid materials: Precision synthesis via α-amino acid *N*-carboxyanhydride polymerization and emerging biomedical applications. *Prog. Polym. Sci.* **2014**, *39* (2), 330−364.

(7) Song, Z.; Han, Z.; Lv, S.; Chen, C.; Chen, L.; Yin, L.; Cheng, J. Synthetic polypeptides: from polymer design to supramolecular assembly and biomedical application. *Chem. Soc. Rev.* **2017**, *46* (21), 6570−6599.

(8) Rasines Mazo, A.; Allison-Logan, S.; Karimi, F.; Chan, N. J.-A.; Qiu, W.; Duan, W.; O'Brien-Simpson, N. M.; Qiao, G. G. Ring opening polymerization of α-amino acids: advances in synthesis, architecture and applications of polypeptides and their hybrids. *Chem. Soc. Rev.* **2020**, *49* (14), 4737−4834.

(9) Bonduelle, C. Secondary structures of synthetic polypeptide polymers. *Polym. Chem.* **2018**, *9* (13), 1517−1529.

(10) Song, Z.; Fu, H.; Wang, R.; Pacheco, L. A.; Wang, X.; Lin, Y.; Cheng, J. Secondary structures in synthetic polypeptides from *N*-carboxyanhydrides: design, modulation, association, and material applications. *Chem. Soc. Rev.* **2018**, *47* (19), 7401−7425.

(11) Li, N.; Lei, Y.; Song, Z.; Yin, L. Helix-specific properties and applications in synthetic polypeptides. *Curr. Opin. Solid State Mater. Sci.* **2023**, *27* (5), No. 101104.

(12) McKinnon, A. J.; Tobolsky, A. V. Structure and properties of poly-γ-benzyl-$_L$-glutamate cast from dimethylformamide. *J. Phys. Chem.* **1968**, *72* (4), 1157−1161.

(13) Watanabe, T.; Tsujita, Y.; Uematsu, I. Influence of casting conditions on the structure of poly(γ-benzyl-$_L$-glutamate). *Polym. J.* **1975**, *7*, 181−185.

(14) Watanabe, J.; Imai, K.; Gehani, R.; Uematsu, I. Structural differences between two crystal modifications of poly(γ-benzyl $_L$-glutamate). *J. Polym. Sci., Polym. Phys. Ed.* **1981**, *19* (4), 653−665.

(15) Fukuzawa, T.; Uematsu, I.; Uematsu, Y. Physical properties of mixtures of poly(γ-benzyl-$_L$-glutamate) and poly(γ-benzyl-$_D$-glutamate). *Polym. J.* **1974**, *6*, 537−541.

(16) Fukuzawa, T.; Uematsu, I.; Uematsu, Y. Viscoelastic properties of poly(γ-benzyl glutamate). *Polym. J.* **1974**, *6*, 431−437.

(17) Samulski, E. T.; Tobolsky, A. V. Distorted α-helix for poly(γ-benzyl $_L$-glutamate) in the nematic solid state. *Biopolymers* **1971**, *10* (6), 1013−1019.

(18) Samulski, E. T.; Tobolsky, A. V. Solid "liquid crystal" films of poly-γ-benzyl-$_L$-glutamate. *Nature* **1967**, *216* (5119), 997.

(19) Samulski, E. T.; Tobolsky, A. V. Some unusual properties of poly(γ-benzyl $_L$-glutamate) films cast in strong magnetic fields. *Macromolecules* **1968**, *1* (6), 555−557.

(20) Nakiri, T.; Imoto, K.; Ishizuka, M.; Okamoto, S.; Date, M.; Uematsu, Y.; Fukada, E.; Tajitsu, Y. Piezoelectric characteristics of polymer film oriented under a strong magnetic field. *Jpn. J. Appl. Phys.* **2004**, *43*, 6769−6774, DOI: 10.1143/JJAP.43.6769.

(21) Deming, T. J. Facile synthesis of block copolypeptides of defined architecture. *Nature* **1997**, *390* (6658), 386−389.

(22) Aliferis, T.; Iatrou, H.; Hadjichristidis, N. Living polypeptides. *Biomacromolecules* **2004**, *5* (5), 1653−1656.

(23) Minich, E. A.; Nowak, A. P.; Deming, T. J.; Pochan, D. J. Rod-rod and rod-coil self-assembly and phase behavior of polypeptide diblock copolymers. *Polymer* **2004**, *45* (6), 1951−1957.

(24) Lu, H.; Cheng, J. Hexamethyldisilazane-mediated controlled polymerization of α-amino acid *N*-carboxyanhydrides. *J. Am. Chem. Soc.* **2007**, *129* (46), 14114−14115.

(25) Habraken, G. J. M.; Peeters, M.; Dietz, C. H. J. T.; Koning, C. E.; Heise, A. How controlled and versatile is *N*-carboxy anhydride (NCA) polymerization at 0 °C? Effect of temperature on homo-, block- and graft (co)polymerization. *Polym. Chem.* **2010**, *1* (4), 514−524.

(26) Baumgartner, R.; Fu, H.; Song, Z.; Lin, Y.; Cheng, J. Cooperative polymerization of α-helices induced by macromolecular architecture. *Nat. Chem.* **2017**, *9*, 614−622.

(27) Wu, Y.; Zhang, D.; Ma, P.; Zhou, R.; Hua, L.; Liu, R. Lithium hexamethyldisilazide initiated superfast ring opening polymerization of alpha-amino acid *N*-carboxyanhydrides. *Nat. Commun.* **2018**, *9*, 5297.

(28) Zhao, W.; Lv, Y.; Li, J.; Feng, Z.; Ni, Y.; Hadjichristidis, N. Fast and selective organocatalytic ring-opening polymerization by fluorinated alcohol without a cocatalyst. *Nat. Commun.* **2019**, *10*, 3590.

(29) Grazon, C.; Salas-Ambrosio, P.; Ibarboure, E.; Buol, A.; Garanger, E.; Grinstaff, M. W.; Lecommandoux, S.; Bonduelle, C. Aqueous ring-opening polymerization-induced self-assembly (ROPISA) of *N*-carboxyanhydrides. *Angew. Chem., Int. Ed.* **2020**, *59* (2), 622−626.

(30) Tian, Z. Y.; Zhang, Z.; Wang, S.; Lu, H. A. moisture-tolerant route to unprotected α/β-amino acid *N*-carboxyanhydrides and facile synthesis of hyperbranched polypeptides. *Nat. Commun.* **2021**, *12*, 5810.

(31) Hu, Y.; Tian, Z.-Y.; Xiong, W.; Wang, D.; Zhao, R.; Xie, Y.; Song, Y.-Q.; Zhu, J.; Lu, H. Water-assisted and protein-initiated fast

and controlled ring-opening polymerization of proline *N*-carboxyanhydride. *National Science Review* **2022**, *9* (8), No. nwac033.
(32) Lv, W.; Wang, Y.; Li, M.; Wang, X.; Tao, Y. Precision synthesis of polypeptides via living anionic ring-opening polymerization of *N*-carboxyanhydrides by tri-thiourea catalysts. *J. Am. Chem. Soc.* **2022**, *144* (51), 23622−23632.
(33) Wang, W.; Fu, H.; Lin, Y.; Cheng, J.; Song, Z. Cooperative Covalent Polymerization of N-carboxyanhydrides: from Kinetic Studies to Efficient Synthesis of Polypeptide Materials. *Accounts of Materials Research* **2023**, *4* (7), 604−615.
(34) Yang, T.; Xue, T.; Mao, J.; Chen, Y.; Tian, H.; Bartolome, A.; Xia, H.; Yao, X.; Kumar, C. V.; Cheng, J.; Lin, Y. Tailoring Synthetic Polypeptide Design for Directed Fibril Superstructure Formation and Enhanced Hydrogel Properties. *J. Am. Chem. Soc.* **2024**, DOI: 10.1021/jacs.3c10762.
(35) Zimm, B. H.; Bragg, J. K. Theory of the phase transition between helix and random coil in polypeptide chains. *J. Chem. Phys.* **1959**, *31* (2), 526−535.
(36) Schellman, J. A. The factors affecting the stability of hydrogen-bonded polypeptide structures in solution. *J. Phys. Chem.* **1958**, *62* (12), 1485−1494.
(37) Qian, H.; Schellman, J. A. Helix-coil theories: A comparative study for finite length polypeptides. *J. Phys. Chem.* **1992**, *96* (10), 3987−3994.
(38) Papadopoulos, P.; Floudas, G.; Klok, H. A.; Schnell, I.; Pakula, T. Self-assembly and dynamics of poly(γ-benzyl-$_L$-glutamate) peptides. *Biomacromolecules* **2004**, *5* (1), 81−91.
(39) Floudas, G.; Spiess, H. W. Self-assembly and dynamics of polypeptides. *Macromol. Rapid Commun.* **2009**, *30* (4−5), 278−298.
(40) Wang, J.; Lu, H.; Ren, Y.; Zhang, Y.; Morton, M.; Cheng, J.; Lin, Y. Interrupted helical structure of grafted polypeptides in brush-like macromolecules. *Macromolecules* **2011**, *44* (22), 8699−8708.
(41) Ren, Y.; Baumgartner, R.; Fu, H.; van der Schoot, P.; Cheng, J.; Lin, Y. Revisiting the helical cooperativity of synthetic polypeptides in solution. *Biomacromolecules* **2017**, *18* (8), 2324−2332.
(42) Ren, Y.; Fu, H.; Baumgartner, R.; Zhang, Y.; Cheng, J.; Lin, Y. Folding cooperativity of synthetic polypeptides with or without "tertiary" interactions. *ACS Macro Lett.* **2017**, *6* (7), 733−737.
(43) Love, J. A.; Morgan, J. P.; Trnka, T. M.; Grubbs, R. H. A practical and highly active ruthenium-based catalyst that effects the cross metathesis of acrylonitrile. *Angew. Chem., Int. Ed.* **2002**, *41* (21), 4035−4037.
(44) Baumgartner, R.; Kuai, D.; Cheng, J. Synthesis of controlled, high-molecular weight poly($_L$-glutamic acid) brush polymers. *Biomaterials science* **2017**, *5* (9), 1836−1844.
(45) Elliott, A.; Fraser, R. D. B.; Macrae, T. P. The X-ray diffraction patterns of poly-γ-benzyl-glutamate. *J. Mol. Biol.* **1965**, *11* (4), 821−828.
(46) Miyazawa, T.; Blout, E. R. The infrared spectra of polypeptides in various conformations: Amide I and II bands. *J. Am. Chem. Soc.* **1961**, *83* (3), 712−719.
(47) Parry, D. A. D.; Elliott, A. The structure of a paracrystalline phase of poly-γ-benzyl-L-glutamate in dimethylformamide. *J. Mol. Biol.* **1967**, *25* (1), 1−13.
(48) Aritake, T.; Tsujita, Y.; Uematsu, I. Structure and properties of precipitates of poly(γ-benzyl glutamate). *Polym. J.* **1975**, *7* (1), 21−25.
(49) Liu, Z.; Li, X.; Zheng, Y.; Wang, S. Q.; Tsige, M. Chain network: Key to the ductile behavior of polymer glasses. *Macromolecules* **2018**, *51* (5), 1666−1673.
(50) Razavi, M.; Wang, S. Q. Why is crystalline poly(lactic acid) brittle at room temperature? *Macromolecules* **2019**, *52* (14), 5429−5441.
(51) Pakula, T.; Zhang, Y.; Matyjaszewski, K.; Lee, H. i.; Boerner, H.; Qin, S.; Berry, G. C. Molecular brushes as Super-soft elastomers. *Polymer* **2006**, *47* (20), 7198−7206.
(52) Dalsin, S. J.; Hillmyer, M. A.; Bates, F. S. Linear rheology of polyolefin-based bottlebrush polymers. *Macromolecules* **2015**, *48* (13), 4680−4691.
(53) Neugebauer, D.; Zhang, Y.; Pakula, T.; Sheiko, S. S.; Matyjaszewski, K. Densely-Grafted and Double-Grafted PEO Brushes via ATRP. *A Route to Soft Elastomers. Macromolecules* **2003**, *36* (18), 6746−6755.
(54) Daniel, W. F. M.; Burdyńska, J.; Vatankhah-Varnoosfaderani, M.; Matyjaszewski, K.; Paturej, J.; Rubinstein, M.; Dobrynin, A. V.; Sheiko, S. S. Solvent-free, supersoft and superelastic bottlebrush melts and networks. *Nat. Mater.* **2016**, *15* (2), 183−189.
(55) McCormick, H. W.; Brower, F. M.; Kin, L. The effect of molecular weight distribution on the physical properties of polystyrene. *J. Polym. Sci.* **1959**, *39* (135), 87−100.

https://doi.org/10.1021/acs.macromol.3c02005
Macromolecules 2024, 57, 2008−2018